ALTEX preprint
published October 23, 2019
doi:10.14573/altex.1906253

Research Article

Development of an *Ex Vivo* Aneurysm Model for Vascular Devices Testing

Noemi Vanerio[1,2], Marco Stijnen[1], Bas A. J. M. de Mol[2], Linda M. Kock[1,3]
[1]LifeTec Group BV, Eindhoven, The Netherlands; [2]Department of Cardiothoracic Surgery and Cardiovascular Sciences, Amsterdam University Medical Center, Amsterdam, The Netherlands; [3]Department of Biomedical Engineering, Eindhoven University of Technology, Eindhoven, The Netherlands

Abstract
An *ex vivo* aneurysm model that closely resembles the *in vivo* situation can provide an important tool for testing therapies. The model should mimic a variety of conditions, such as *in vivo* hemodynamics and native arterial structure and characteristics, avoiding animal experimentation. Therefore, the aim of this study is to develop an *ex vivo* aneurysm model by vessel wall stiffening to be used to assess treatment strategies. Porcine carotid arteries from slaughterhouse animals were used to evaluate the acute effect of different concentrations of Rose Bengal on distensibility. This sono-sensitive compound was activated by several ultrasound frequencies, resulting in stiffening of the treated arteries of which the most effective combination was selected. In a pulsatile *ex vivo* vascular bioreactor treated and control porcine carotid arteries were subjected to physiological conditions for 10 days. During culture, hemodynamics showed increased mean pressure and decreased pulsatility in treated arteries compared to controls. Change in vessel morphology and significant increase of distal diameter was observed in the treated arteries but not in the controls. Histology of treated arteries revealed dissection-like lesions distally and aneurysm-like structure proximally. Finally, a stent graft was deployed in one treated artery and cultured demonstrating the feasibility of testing endovascular devices in the model. In conclusion, we developed an *ex vivo* model reproducing the onset of aneurysm formation. This could represent a promising tool for early stage device testing thereby reducing the need for animal studies.

1 Introduction

Abdominal aortic aneurysm (AAA) is a life-threatening and often asymptomatic cardiovascular disease consisting of an abnormal dilation of the aorta characterized by vessel wall weakening, which develops until rupture. The prevalence of AAA is ≈ 5 % in men and ≈ 1 % in women above 60 years old (Golledge and Norman, 2011); its rupture carries a 90% overall mortality (Giugliano et al., 2018; Upchurch and Criado, 2009).

The etiology and pathogenesis of aneurysms are poorly understood. It seems that aneurysm formation is associated with a significant increase in stiffness of the arterial wall compared to healthy tissue in both AAA (He and Roach, 1994; MacSweeney et al., 1992; Sonesson et al., 1997; Vande Geest et al., 2006) and cerebral aneurysms (Robertson et al., 2015). Mechanical properties of the arterial wall, such as stiffness, are dependent on extracellular matrix composition, particularly on the amount, orientation and crosslinks of elastin and collagen fibers (Gasser et al., 2012). In fact, reduction and degradation of elastin in end-stage AAA have shown to stimulate aneurysm development (Campa et al., 1987; Carmo et al., 2002; Isenburg et al., 2007) and therefore loss of elastin is believed to be the main characteristic of aneurysms. In the last years, aneurysm development has been increasingly related to impaired collagen homeostasis (Lindeman et al., 2010). Studies based on the analyses of collagen content in AAA tissue showed discordant results, observing decrease (McGee et al., 1991), increase (He and Roach, 1994; Rizzo et al., 1989) or no changes (Gandhi et al., 1994) in collagen content. Conversely, collagen crosslinking has shown to be increased in AAA (Carmo et al., 2002; Lindeman et al., 2010; Wågsäter et al., 2013) and alterations in collagen microarchitecture in AAA and Marfan's syndrome tissue resulted in tissue mechanical failure (Lindeman et al., 2010). However, the exact role of collagen in aneurysm pathophysiology and whether the loss of elastin function or collagen crosslink or their combination trigger the pathology are still unknown. To optimize treatments and better understand aneurysm pathophysiology, several *in vivo* animal models have been developed over the years to mimic aneurysm onset, progression and rupture. In papers by Patelis et al. (Patelis et al., 2017) and Lysgaard Poulsen et al. (Lysgaard Poulsen et al., 2016) the main *in vivo* models of AAA are reviewed, underlining the high number of animal models used for this purpose. In rodent animal

Received June 25, 2019; Accepted October 21, 2019;
Epub October 23, 2019;

ALTEX 37(#), ###-###. doi:10.14573/altex.1906253

Correspondence: Linda M. Kock, PhD,
LifeTec Group BV, Kennedyplein 10-11,
5611 ZS Eindhoven, The Netherlands
(l.kock@lifetecgroup.com)

models, aneurysms are induced by using porcine pancreatic elastase (Mao et al., 2015; Nuki et al., 2009), calcium chloride infusion (Isenburg et al., 2007), implantation of xenografts, angiotensin II infusion in knockout mice (Trachet et al., 2016) or by creating transgenic models (Lysgaard Poulsen et al., 2016). These models have good reproducibility, elastase leads to fast dilatation, calcium chloride and angiotensin II models induce aneurysms without arterectomy and, in the xenograft models, formation of intraluminal thrombus is commonly obtained. However, all these models require major surgery and are technically difficult in addition to being time consuming, costly and not suitable for device testing because of the different size and morphology (Lysgaard Poulsen et al., 2016). Therefore, these models are mainly used for understanding of pathological mechanisms. For interventional testing, non-rodent larger animal models were first introduced. In these models, aneurysms are mainly induced chemically with elastase, collagenase (or combinations of both) (Czerski et al., 2013) or calcium chloride or mechanically by using grafts or patches (Lysgaard Poulsen et al., 2016). In the chemically induced models, aneurysm formation is achieved in terms of elastin disruption and diameter dilatation only when combination of elastase, collagenase and angioplasty are used. Lack of long-term results require more research on these models. In the mechanical aneurysm models, anatomical characteristics can be reproduced and some pathological similarities were found, but no further enlargement of the aneurysm can be obtained.

In addition to the limitations of the rodent and non-rodent animal models above mentioned, obviously, the use of *in vivo* animal models implies ethical issues, time- and money-consuming protocols, high complexity of the model and poor controllability of the experiments. In this perspective and considering the 3R's principle, *ex vivo* aneurysm models using slaughterhouse tissue could be a valuable alternative and would replace *in vivo* animal models (Lysgaard Poulsen et al., 2016; Patelis et al., 2017), overcoming limitations and disadvantages of *in vivo* studies while including biological response and physiological environment which is limited or absent in *in vitro* testing. Moreover, *ex vivo* aneurysm models could provide a tool to study aneurysms at early phases of the disease that is usually not possible since tissue is harvested after aneurysm rupture. Recently, a number of *ex vivo* aneurysm models have been developed. In one of these models, PTFE grafts were dilated to create an aneurysmal scaffold, seeded with stromal vascular fraction cells and cultured in a bioreactor for 14 days (Touroo and Williams, 2012). The development of a tissue-engineered aneurysm model was supported by the formation of a layer of smooth muscle cells. This model could be used as testing platform for endovascular devices, however the lack of native tissue is a limitation because of the absence of actual tissue composition, structure and biomechanical properties. Another study focussed on the phenotype of smooth muscle cells (SMCs) isolated from porcine carotid arteries that were treated with collagenase and elastase and cultured in a steady flow bioreactor for 12 days (Riches et al., 2013). Phenotype of the isolated SMCs showed changes comparable to end-stage AAA samples in terms of rhomboid morphology, increased spread area and senescence and impaired proliferation. This approach allows for SMCs dysfunction studies especially focusing on early stage aneurysm development. On the other hand, absence of physiological pulsatile hemodynamics and not significant diameter changes were reported.

Due to the limitations of the other *ex vivo* models, we consider that an *ex vivo* model of aneurysm that closely resembles the *in vivo* situation and conditions, such as *in vivo* hemodynamics and native blood vessel structure and characteristics, is still missing.

Therefore, the aim of this study is to develop a novel *ex vivo* aneurysm model. This has been based on stiffening and subsequently culturing of porcine carotid arteries. It has been shown that the pathogenesis and etiology of aneurysms are only minimally dependent on the location of the vasculature (Tanweer et al., 2014). Due to the similarities in structure and characteristics between the aortic and carotid wall and because carotid arteries are considered good models of AAA in other *ex vivo* (Riches et al., 2013) and *in vivo* (Patelis et al., 2017) experiments, carotid arteries were used in this study.

It has been shown that stiffening of biological tissues can be induced experimentally by using photochemical-based processes using for example Rose Bengal (RB), a xanthene dye which can be activated by green light or ultrasound (Bekesi et al., 2017; Cherfan et al., 2013; Salinas et al., 2017; Xu et al., 2015). Upon activation, Rose Bengal can create covalent bonding of structural proteins such as crosslinks in collagen molecules leading to tissue stiffening. Therefore, a treatment consisting of RB activated by ultrasound is assessed in this study for its ability to induce arterial wall stiffening and ultimately aneurysm formation. First, the acute effect of different concentrations of Rose Bengal in combination with different ultrasound frequencies on the mechanical properties of native porcine carotid arteries is evaluated in order to select the most optimal combination. Second, the achievement of aneurysm formation is evaluated in terms of long-term response of carotid arteries to Rose Bengal-ultrasound treatment in the pulsatile *ex vivo* vascular bioreactor. Finally, to demonstrate the feasibility of testing endovascular devices in the platform and to assess whether the device has influence on the further development of the aneurysm formation, a pilot study is performed in which a stent graft is implanted in a treated carotid artery cultured in the *ex vivo* vascular bioreactor.

2 Materials and methods

All porcine common carotid arteries used in the experiments were obtained from Dutch Landrace pigs 5-7 months old weighing 100-110 kg from a local slaughterhouse, following the routine slaughtering procedure. Each carotid artery was obtained from a different pig.

2.1 Acute effect of Rose Bengal-ultrasound treatment on arterial distensibility

2.1.1. Carotid artery preparation

In the slaughterhouse, the carotid arteries were immediately flushed after dissection with phosphate-buffered saline (PBS, Sigma-Aldrich, Zwijndrecht, The Netherlands) at 4 °C to remove blood and were subsequently stored in PBS on ice until their arrival in the laboratory within 1 hour after slaughter. Upon arrival, the carotid arteries were trimmed to remove the surrounding connective tissue, while submerged in cold PBS.

2.1.2. Experimental groups

Prepared carotid arteries (n ≥ 3 per group) were divided into 8 groups (Tab. 1). Each artery underwent distensibility testing within 3 hours from isolation and was then treated with Rose Bengal and/or ultrasound. Distensibility testing was repeated within 1 hour on the treated arteries to evaluate the effect of the Rose Bengal-ultrasound treatment. In each group, a different combination of Rose Bengal concentration ([RB]) and ultrasound (US) frequency was used (Tab. 1). The chosen concentrations of Rose Bengal have been previously reported as non-cytotoxic in photochemical tissue bonding applications (Barton et al., 2012; Xu et al., 2015). The clinically most used and easily available ultrasound frequencies were selected for testing. The paired control, named untreated, consisted of PBS which did not undergo sonication (combination of 0 % RB concentration and no sonication namely 0 MHz US frequency).

		US frequency		
		0 MHz	**3.5 MHz**	**7.5 MHz**
[RB]	**0 %**	untreated	RB0US3.5 (control)	RB0US7.5 (control)
	0.1 %	RB0.1US0 (control)	RB0.1US3.5	RB0.1US7.5
	1 %	RB1US0 (control)	RB1US3.5	RB1US7.5

Tab. 1: **Experimental groups for testing the acute effect of Rose Bengal-ultrasound treatment on arterial distensibility**: combination of RB concentrations and US frequencies.

2.1.3. Rose Bengal-ultrasound treatment

Rose Bengal-ultrasound treatment consisted of infusion of Rose Bengal solution inside the arteries followed by ultrasound activation. Rose Bengal (Rose Bengal sodium salt, Dye content 95 %, Sigma-Aldrich, Zwijndrecht, The Netherlands) solutions at concentration of 0.1 % and 1 % w/v of PBS were prepared. Carotid arteries were mounted proximally and distally in a support chamber and filled with RB solution using a 10 ml syringe without needle (BD Plastipak™, Fisher Scientific, Landsmeer, The Netherlands) and RB solution was allowed to diffuse into the vessel wall. After 3 minutes, the vessel underwent sonication treatment for 2 minutes, using an ultrasound machine (SSD-2000, Aloka, Tokyo, Japan) equipped with 3.5 or 7.5 MHz probe.

2.1.4. Distensibility testing protocol

Mechanical properties of the untreated and treated porcine carotid arteries were evaluated and compared in terms of distensibility. Each artery was mounted on connectors in a dedicated setup and stretched to 150 %, which is the physiological pre-stretch of porcine carotid arteries *in vivo* (Boekhoven et al., 2014). The artery was maintained at room temperature in a PBS bath during the test. Fixed volumes of PBS were injected with a syringe at 0.1 ml/s until reaching a pressure of around 160 mmHg. Pressure values inside the artery were recorded by a pressure transducer (BD P10EZ, Becton Dickinson, Sandy, Utah, USA) and the signal was transmitted to a PC through a pressure amplifier (Picas, Peekel Instruments BV, Rotterdam, The Netherlands) and a breakout box (NI BNC-2090, National Instruments, Austin, Texas, USA). At the end of the test on the untreated artery, Rose Bengal-ultrasound treatment was performed on the vessel while mounted in the vessel chamber of the setup. The distensibility test was then repeated on the treated carotid artery following the same protocol.

2.1.5. Data analysis and statistics

Distensibility of the arteries was analysed by comparing the normalized change in volume (compared to initial volume of fluid present in the artery) and the hydrostatic pressure measured. Distensibility values represent the slope of the normalized volume versus hydrostatic pressure curve, for physiological pressure values at or above 90 mmHg. Data was expressed as mean ± SEM. Two-tailed paired Student's t-test was used to analyse distensibility differences between untreated and treated arteries and $P < 0.05$ was considered statistically significant.

2.2 Long-term response of carotid arteries to Rose Bengal-ultrasound treatment

2.2.1 Carotid artery preparation

In the slaughterhouse, harvested porcine common carotid arteries (n = 8) were directly flushed with ice-cold sterile modified Krebs solution (Krebs-Henseleit solution supplemented with 10^{-1} mM papaverine (Sigma Aldrich, St. Louis, MO, USA), 0.05 mM 2-mercaptoethanol (Gibco™, LifeTechnologies, Bleiswijk, The Netherlands), 2% antibiotic penicillin-streptomycin (10,000 U/mL, Gibco™), 0.6% antimycotic amphotericin B (0.75 ng/mL, Gibco™)) and transported immediately afterwards to the lab in sterile jars on ice containing modified Krebs solution. In a laminar flow hood, vessels were gently trimmed to remove excess connective tissue, minimizing damage to the endothelium, and segments of 6 cm length were cut while submerged in fresh cold sterile modified Krebs solution. Half of the prepared vessels (n = 4) were treated with sterile-filtered (0.22 µm, Fisher Scientific, Landsmeer, The Netherlands) 1 % w/v RB solution and 3.5 MHz ultrasound frequency, before placing them in the bioreactor. Previous results showed that this combination is the most effective in stiffening the arterial tissue.

2.2.2 Experimental setup

Porcine carotid arteries (n = 8) were cultured in a pulsatile *ex vivo* vascular bioreactor for 10 days (day 0: start culture, day 9: end culture) under physiological hemodynamics, temperature of 38 °C, 100 % humidity, 5 % CO_2 (Vanerio et al., 2019). The arteries were divided into 2 experimental groups: control group (n = 4), consisting of untreated arteries, and treated group (n =

4) consisting of arteries treated with 1 % Rose Bengal solution and 3.5 MHz ultrasound frequency. During culture, hemodynamic parameters were measured continuously and acquired hourly, while ultrasound imaging was performed daily.

2.2.3 Culture protocol in ex vivo vascular bioreactor

A custom developed *ex vivo* vascular bioreactor, previously described (Vanerio et al., 2019), was used. The *ex vivo* vascular bioreactor consists of a reservoir chamber in which fresh medium is stored, an in-house developed circulation pump that pumps the fresh medium from the reservoir into a first compliance chamber which dampens pressure and flow curves, a vessel culture chamber in which an artery can be placed and a Windkessel model (variable resistance-compliance chamber-variable resistance) to replicate the vascular impedance of the systemic circulation and connected back to the reservoir. Briefly, under a laminar flow hood, the artery was mounted on connectors and positioned in the vessel culture chamber equipped with an ultrasound window for vessel imaging. Culture medium was pumped from the reservoir into the lumen of the artery by the in-house developed pump and pulsatile physiological hemodynamics was set by using the compliance chambers and adjustable resistances. Connection between the reservoir and the vessel culture chamber allowed for external perfusion of the artery. A medium refreshment circuit provided 2 ml/min of fresh medium hourly and automatically.

All arteries were cultured in Dulbecco's modified eagle's medium containing 1 g/L D-glucose, 25 mM HEPES, 1mM pyruvate, 4mM L-glutamine (Gibco™ DMEM, low glucose, pyruvate, HEPES, Gibco, LifeTechnologies, Bleiswijk, The Netherlands) supplemented with 50 µM 2-mercaptoethanol (2-Mercaptoethanol (50 mM) Gibco™), 10% fetal bovine serum (Gibco™), 1% antibiotic penicillin-streptomycin (Penicillin-Streptomycin (10,000 U/mL) Gibco™), antimycotic amphotericin B (0.75 ng/mL, Amphotericin B, Gibco™), vascular endothelial growth factor (VEGF 2.5 ng/mL, PeproTech Inc, Rocky Hill, NJ, USA) and Xanthan gum (0.66 g/L, Fisher Scientific, Landsmeer, The Netherlands) to mimic blood-like viscosity.

Upon start of the culture, physiological longitudinal pre-stretch of 150 % was applied to the arteries. After a warm up phase of 3 hours in which the pressure was gradually increased to 120/80 mmHg, flow rate was set to achieve a physiological shear stress value of 2.4 Pa (Vanerio et al., 2019).

2.2.4 Data analyses

2.2.4.1 Hemodynamics

Pressure values were measured up- and downstream of the vessel using pressure transducers (RT2000 system, Argon Medical Devices Netherlands B.V.) and the flow rate was measured at the inlet of the vessel using an ultrasonic flow sensor (Sono TT and OEM Flow Measurement Board, Em-tec GmbH, Finning, Germany).

2.2.4.2 Ultrasound imaging

An ultrasound machine (Esaote Picus Pro with arterial analyzer Art.Lab, Esaote Europe, The Netherlands) equipped with a linear probe (7.5 MHz acquisition frequency) was used to perform ultrasound imaging. Diameter estimation was achieved upon determination of inner and outer borders of the artery with in house developed software (based on (Loizou et al., 2009)). Shape, straightness and intima-media-adventitia layer structure were qualitatively analyzed from the post-processed ultrasound images.

2.2.4.3 Histology

At the end of the culture, rings of the proximal and distal part of the cultured vessels (n = 4 per group) were cut, embedded in Tissue-Tek O.C.T. Compound (Sakura Finetek USA Inc, Torrance, California, USA) and snap frozen in isopentane solution (2-Methylbutane, Sigma Aldrich, St. Louis, MO, USA). 5 µm-thick sections were cut with a cryostat (SLEE MNT, SLEE medical GmbH, Mainz, Germany), mounted on a glass slide and stained for collagen and elastin, using a commercially available kit (Modified Verhoeff Van Gieson Elastic Stain Kit, Cat. HT25A Sigma Aldrich, St. Louis, MO, USA). All sections were examined under an optical microscope (Eclipse TE300, Nikon) with magnification of 4x and digital pictures (CMEX-3 Digital Microscope Camera DC.3000c, Euromex Microscopen BV, Arnhem, The Netherlands) were taken.

2.2.5 Statistics

To obtain the diameter change, diameter values were normalized to diameter at day 1, which is the timepoint at which the vasoconstriction due to harvesting procedure is recovered, therefore the diameter value is comparable to the *in vivo* condition. Diameter changes were expressed as mean ± SEM. Two-way ANOVA analysis was used to evaluate the influence of time and treatment on diameter. Post-hoc comparisons using Bonferroni correction were used to determine significant differences between groups per timepoint. $P < 0.05$ was considered statistically significant.

2.3 Device assessment - pilot study

A pilot study to assess the feasibility of testing endovascular devices in the *ex vivo* aneurysm model was performed. A porcine carotid artery (n = 1) was cultured in the *ex vivo* vascular bioreactor following the protocol above after treatment with 1 % Rose Bengal solution and 3.5 MHz ultrasound frequency. After the artery was cultured for 6 days, a 5 mm x 12 mm stent graft (Jostent GraftMaster®, Abbott Vascular Inc., Santa Clara, California, USA) was delivered over a guidewire and deployed at 16 atm in the distal segment of the cultured carotid artery under ultrasound guidance. The artery was then further cultured for 4 days to reach a total of 10 days of culture. During culture, hemodynamics data were acquired hourly, ultrasound imaging was performed daily. Histological analyses were performed at the end of the culture.

ALTEX preprint
published October 23, 2019
doi:10.14573/altex.1906253

3 Results

3.1 Effect of Rose Bengal-ultrasound treatment on arterial distensibility

Distensibility of porcine carotid arteries before and after treatment with Rose Bengal and ultrasound was compared by analysing the slope of the normalized volume in the artery versus the hydrostatic pressure curve above 90 mmHg (Fig. 1). Treatment with either only RB without ultrasound activation (RB0.1US0, RB1US0) or by only ultrasound without RB infusion (RB0US3.5, RB0US7.5) did not result in a significant change in distensibility compared to the untreated situation. The distensibility of arteries treated with both RB and ultrasound was significantly decreased compared to the distensibility of the same arteries before treatment, except for the combination of 1 % RB concentration and 7.5 MHz ultrasound frequency, which was not statistically significant. To compare the different groups, distensibility ratio defined as ratio between the distensibility before the treatment and the distensibility after the treatment was calculated. Distensibility ratio of RB1US3.5 group resulted the highest compared to the other groups, although not statistically significant (data not shown).

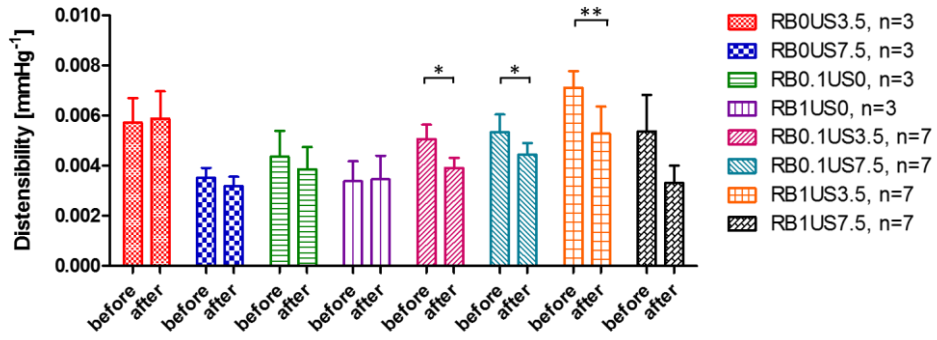

Fig. 1: Distensibility values comparing arteries treated with different combinations of concentrations of Rose Bengal (RB: 0, 0.1, 1 %) and ultrasound frequencies (US: 0, 3.5, 7.5 MHz)
Control groups treated with either RB or ultrasound show no statistically significant difference of distensibility between arteries before and after the treatment. Statistically significant decrease of distensibility is observed in arteries after treatment with both RB and US, with the exception of RB1US7.5. Values are displayed as mean ± SEM. *p < 0.05; **p < 0.001.

3.2 Long-term response of carotid arteries to Rose Bengal-ultrasound treatment

Treated porcine carotid arteries (n = 4, RB 1 % US 3.5 MHz) and untreated control arteries (n = 4) were cultured in the *ex vivo* vascular bioreactor for 10 days, from day 0 to day 9, and compared in terms of hemodynamics, vessel geometry, wall structure and composition. All results showed the same trend besides of one of the treated arteries that is presented separately at the end of the paragraph because of the divergent response that was observed. For the other treated arteries (n = 3) and the untreated controls (n = 4), one cycle (660 s) of pressure curves at the start and at the end of the culture are shown in Fig. 2. At day 2, the pressure curves of the control and treated groups overlap in the pulsatile physiological range of 120/80 mmHg (Fig. 2A). On the contrary, at day 9, the pressure curve of the treated group shows an increased mean pressure and a reduced pulsatility, defined as difference between the maximum and the minimum pressure values, compared to the untreated control group (Fig. 2B), although the pressure curves remain in the physiological range.

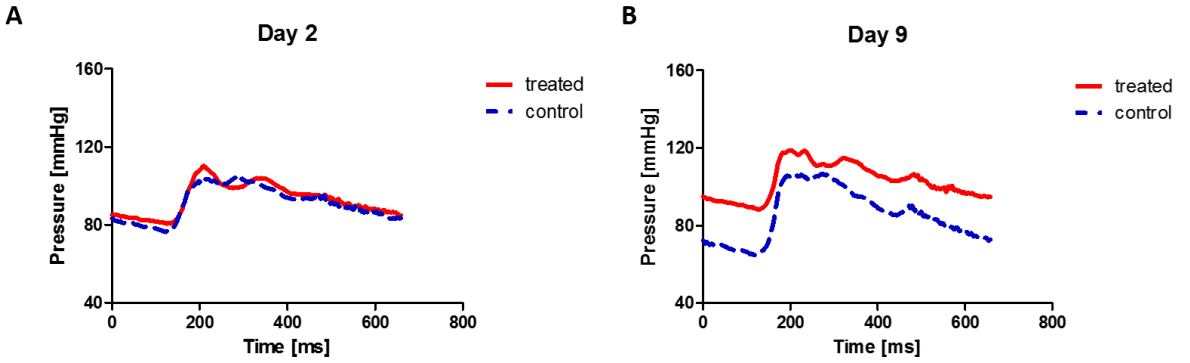

Fig. 2: Pressure curves at day 2 and 9 measured in porcine carotid arteries cultured in the *ex vivo* vascular bioreactor, comparing control group (n = 4) and treated group (n = 3)
(A) No differences are noticeable at day 2 comparing controls with treated arteries. (B) Increase of mean pressure is shown in treated carotids compared to controls at day 9.

ALTEX preprint
published October 23, 2019
doi:10.14573/altex.1906253

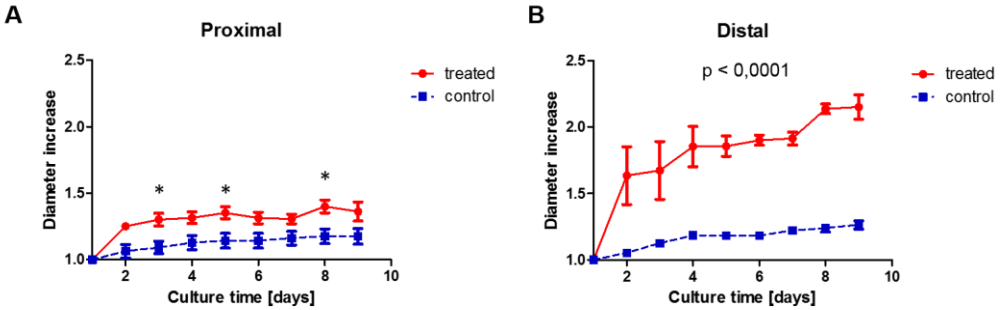

Fig. 3: Diameter change of proximal and distal porcine carotid arteries during culture in the *ex vivo* vascular bioreactor, comparing control group (n = 4) and treated group (n = 3)
(A) Slight difference in increase of proximal diameter in treated arteries compared to controls over time. Statistically significant increase in diameter over time for both control and treated arteries ($p < 0.0001$). (B) Statistically significant difference in increase of distal diameter in treated arteries compared to controls at all timepoints and over time in both control and treated arteries ($p < 0.0001$). Values are displayed as mean ± SEM.

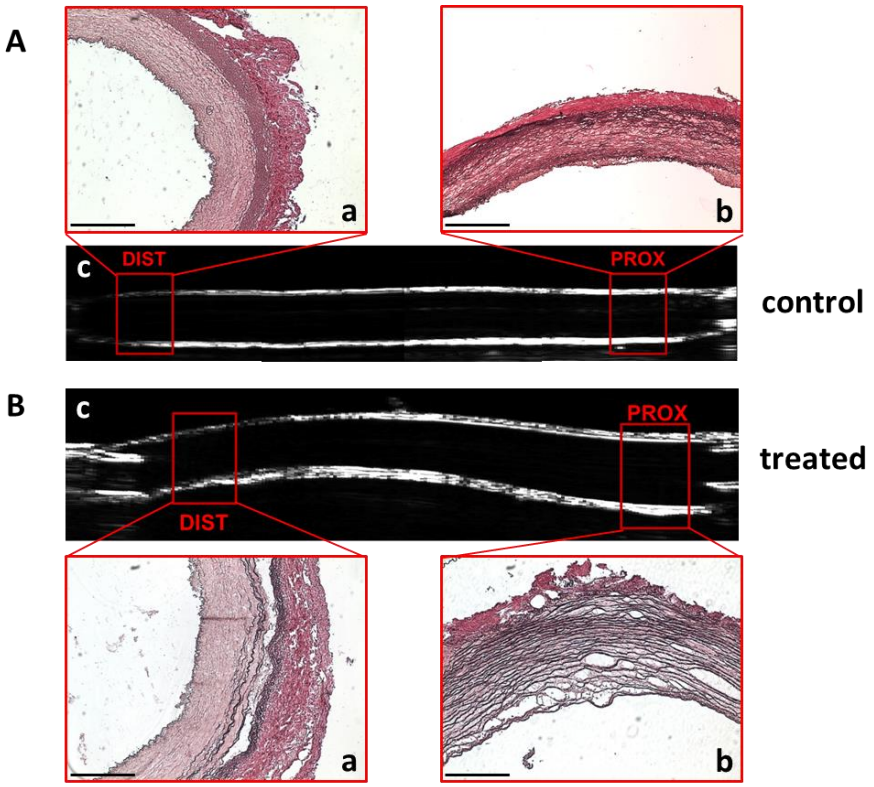

Fig. 4: Histology and ultrasound images of control and treated vessels after 10 days of culture in the *ex vivo* vascular bioreactor
(A) Untreated control arteries: VVG staining shows physiological structure in both (a) distal and (b) proximal segments. (c) Physiological vessel morphology and structure are visible from ultrasound imaging. (B) Treated arteries: Verhoeff-Van Gieson (VVG) staining shows (a) separation of the vessel wall layers in the distal segments and (b) loose wall structure in the proximal segments. (c) Changes in vessels morphology are shown with ultrasound imaging. VVG: Collagen fibers are stained in red, elastin fibers in black; scale bar: 500 µm.

Geometry change of the vessels was evaluated during culture in terms of diameter change of proximal and distal segments of control (n = 4) and treated (n = 3) arteries (Fig. 3). The proximal segments show a statistically significant increase in diameter over time in both treated and control arteries ($p < 0.0001$). Moreover, the diameter of treated arteries is significantly increased compared to control arteries at day 3, 5 and 8, reaching a value of 1.36 (Fig. 3A). In the distal segments (Fig. 3B), increase in diameters is observed over time in both treated and control groups ($p < 0.0001$). The diameter increase of treated arteries is significantly higher (reaching 2.15) compared to the untreated controls (reaching 1.26) at all timepoints ($p < 0.0001$).

Vessel wall structure and composition were analyzed by ultrasound imaging daily and histology was performed at the end of the culture on proximal and distal segments. In Fig. 4, ultrasound and histology images of a representative untreated control (n = 4, Fig. 4A) and a treated (n = 3, Fig. 4B) artery after being cultured for 10 days are shown. VVG staining of untreated control arteries shows that the vessel wall presents a compact structure and physiological extracellular matrix in both distal (Fig. 4A-a) and proximal segments (Fig. 4A-b). Rectilinear morphology and physiological vessel wall structure of control arteries is also visible in ultrasound imaging (Fig. 4A-c). In contrast, in treated arteries VVG staining showed separation of the vessel wall layers and disorganization of the elastin fibers in the distal segments (Fig. 4B-a) and moderate disruption of the extracellular matrix resulting in loose structure with visible spaces between elastin fibers in the proximal segments (Fig. 4B-b). Ultrasound images of the treated vessels display a curvature of the vessel and increased wall thickness (Fig. 4B-c).

A divergent response was observed in one of the treated porcine carotid arteries compared to the other arteries within the same experimental group and to controls, summarized in Fig. S1[1]. In terms of hemodynamics, at the end of the culture, the pressure curve of the divergent treated artery showed a high increase of mean pressure, absence of pulsatility and values of pressure above the physiological range of 120/80 mmHg (Fig. S1A-b[1]) compared to the other treated and untreated arteries. Vessel geometry assessment revealed a significant increase of diameter in both distal (Fig. S1B-a[1]) and proximal segments (Fig. S1B-b[1]). Over time, the vessel lost its straight morphology and separation of the vessel wall layers occurred leading to bulge development (Fig. S1C[1]). VVG staining shows loose wall structure with visible spaces in the distal segment (Fig. S1D-a[1]). Massive disruption of the extracellular matrix and bulge formation is observed close to the proximal segment (Fig. S1D-b[1]). Tissue growth and moderate disruption of the extracellular matrix is visible in the proximal segment (Fig. S1D-c[1]).

3.3 Device assessment - pilot study

A stent graft was successfully implanted in the distal part of a treated carotid artery at day 6 and cultured for subsequent 4 days in the *ex vivo* vascular bioreactor. Elastin and collagen VVG staining shows compact and overall regular extracellular matrix structure and fragments of the stent graft in the distal segment (Fig. 5A-a), compact and regular tissue structure in the middle segment (Fig. 5A-b) and presence of empty spaces and elastin disruption in the extracellular matrix of the proximal segment (Fig. 5A-c). At day 9, ultrasound imaging displays the presence of the stent graft in the distal part, straight morphology and physiological vessel wall layer structure predominantly (Fig. 5B). In Fig. 5C, the stent graft implanted in the carotid artery is reported. No macroscopic response of the vessel to the stent was noticed.

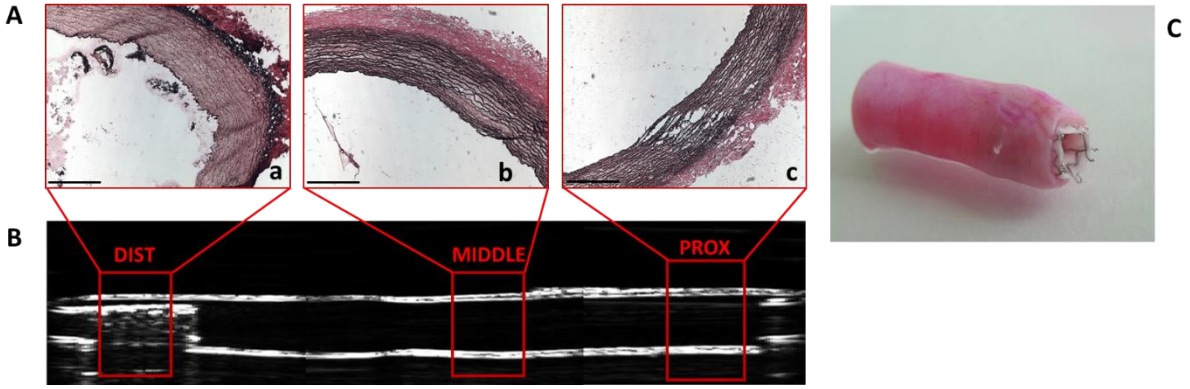

Fig. 5: Stent graft implanted in the *ex vivo* aneurysm model
(A) VVG staining shows compact structure and stent fragments in the distal (a), physiological structure in the middle (b) and damage of the extracellular matrix in proximal (c) segments. (B) Physiological morphology and stent graft implanted in the distal segment, visible with ultrasound imaging at day 9. (C) Carotid artery with implanted stent graft at the end of the culture. VVG: Collagen fibers are stained in red, elastin fibers in black; scale bar: 500 µm.

4 Discussion

In this study, we developed a novel *ex vivo* aneurysm-like model by wall stiffening of cultured native carotid arteries with sono-activated Rose Bengal. First, the immediate effect of different combinations of sono-activated Rose Bengal on the mechanical properties of porcine carotid arteries was investigated. The distensibility values of the tested carotid arteries were comparable to values previously reported (Roy et al., 2005). A possible explanation of the observed differences in distensibility of the vessels comparing all groups before treatment could be ascribed to inter-subject variability. A statistically significant decrease of distensibility was observed in arteries that were treated with both Rose Bengal and ultrasound. To our knowledge, this is the first study showing that sono-activated RB can be used to stiffen biological tissues. A similar effect was already established using RB in combination with photo-activation, for example in photochemical tissue bonding applications (Cherfan et al., 2013; Lauto et al., 2010; O'Neill et al., 2007; Vanerio et al., 2019). In photochemical tissue bonding, the reaction between RB and green light causes covalent bonding of structural proteins leading to crosslinking of collagen molecules. In our case, sono-activation instead of photo-activation was proposed to avoid the use of green light sources which are costly, more invasive and require safety measures (Vanerio et al., 2019). Our finding supports the hypothesis that photo- and sono-activation of RB may induce similar reactions and mechanisms leading to similar stiffening outcomes, eventually. Although the precise mechanism of interaction between ultrasound and sono-sensitizers (e.g. Rose Bengal) is unknown, other studies suggested that cavitation caused by ultrasound induces chemical activation of sono-sensitizers leading to free radicals formation (Hiraoka et al., 2006; Nakonechny et al., 2013). Free radicals can react with amino acids, which can trigger crosslinking of collagen fibers, similarly to what is observed in Rose Bengal photoactivation. The lack of change in distensibility when one of the parameters (ultrasound or Rose Bengal) is absent demonstrates that sono-activation and consequent stiffening take place only when both stimuli are present. Lower RB concentrations seem to lead to lower distensibility decrease, which could be explained by having less RB in the vessel wall available for collagen crosslinking. The combination RB1US3.5 has been selected for the long-term culturing studies because it showed the most significant decrease in distensibility. It is not clear why the combination RB1US7.5 showed

[1] doi:10.14573/altex.1906253s

a non-significant decrease of distensibility. Since a higher US frequency is characterized by lower tissue penetration depth, this might have led to only partial activation of RB and consequently to lower collagen crosslinking resulting in lower decrease of distensibility. To test whether this is the mechanism that is involved in the stiffening of the vessel wall, quantification of collagen crosslinking needs to be performed.

In a next study, porcine carotid arteries were treated with sono-activated RB and subsequently cultured for 10 days in a vascular bioreactor. The stiffening induced by the sono-activated RB treatment, which is a characteristic present in aneurysms, is tested in long-term settings with the aim of creating an *ex vivo* aneurysm model.

At the end of the culture, treated arteries showed a slightly higher mean pressure and lower pulsatility compared to controls, which was very pronounced in the divergent treated artery (Fig. 5). This increase of mean pressure could possibly be caused by a narrowing of the lumen of the tubes downstream the artery because of accumulation of detached cells or because of increase of medium viscosity due to the possible secretum of the smooth muscle cells, although no blockage was observed. The decrease of pulsatility in the treated vessels can be considered a consequence of dilation of the vessels, as at similar flow rate, the relative volume increase in the vessel during a single stroke contributes less to the total artery volume when the artery is already dilated. The ratio between the volume of the single stroke and the maximum artery volume is lower for higher artery volume, resulting in smoothening of the pressure curves. The main distinctive characteristic of aneurysms is arterial dilation which is considered to be aneurysmal when the artery diameter reaches 150% of the original diameter (Johnston et al., 1991; Nordon et al., 2011). In our untreated control vessels, a small increase, below 150%, in diameter over time was observed, which is probably caused by adaptation of the vessel to the new environment. Conversely, treated vessels showed increases in diameter exceeding 150%, especially in distal segments already after 3 days of culture. In the divergent vessel, both proximal and distal diameter increases reached values of 200 % and almost 300 % for proximal and distal segments, respectively.

The aneurysm-like pathological appearance of the treated arteries is supported by ultrasound imaging and histological findings. Untreated control vessels showed physiological morphology while treated vessels showed curved morphology, probably due to extracellular matrix damage which can lead to elongation and consequent curvature. Elastin and collagen play a role in retaining tissue structure and therefore alterations in their networks can lead to changes in the morphology. The pronounced s-shaped morphology of the divergent vessel visible on the ultrasound images could possibly be attributed to buckling because of the high-pressure values in the artery. Moreover, in the same vessel a noticeable bulging with delamination of the layers was observed resembling dissection and aneurysm-like lesions *in vivo*. Nevertheless, ultrasound images of carotid arteries cultured in the *ex vivo* vascular bioreactor cannot directly be translated and compared to ultrasound images taken *in vivo*. This is because *in vivo* the arteries are surrounded by tissue which limits the displacement or the curvature of the artery during the progression of the pathology, while in *ex vivo* systems, where no surrounding tissue is present, displacement and curvature can occur.

Elastin and collagen staining confirmed the ultrasound evidences by showing delamination of vessel wall layers distally and loose extracellular matrix structure in the proximal segments of the treated vessels. Histology of the cultured treated arteries presented several similarities to *in vivo* human and animal aneurysmal tissue. The observed distal separation of vessel wall layers can be related to dissection lesions in humans and animals (Chen et al., 2009). The proximal loose structure of the extracellular matrix with numerous lacunae may reveal disruption, fragmentation and degeneration of elastin fibers as displayed in aneurysms and dissections in *in vivo* animal models (Isenburg et al., 2007; Li et al., 2016; Ren et al., 2016) and human biopsies (Chen et al., 2009). In the divergent treated vessel presenting bulge formation, extracellular matrix in correspondence with the bulging segment resulted majorly disrupted. A difference that is noticeable when comparing *in vivo* aneurysm and dissection histology with treated arteries is the absence of thrombus due to the fact that no blood is involved in our *ex vivo* model.

The stiffening treatment was applied to the entire vessel leading to significant increase of the distal diameter and in one case to severe enlargement of both proximal and distal diameters. In all treated vessels, histological analyses showed differences in aneurysm and dissection-like characteristics between proximal and distal segments. It is known that mechanical properties, extracellular matrix composition and passive behavior of carotid arteries differ when comparing proximal and distal segments (García et al., 2012; Sokolis et al., 2011). We speculate that the reason why aneurysm-like lesions are located in the proximal segments is related to the elastic nature of the segment, while dissection-like lesions are located mostly in the distal parts due to the muscular nature of the part. However, the specific influence of the different vessels segments on pathology progression is unclear, specifically it is unknown whether this influence can be ascribed mainly to the passive viscoelastic mechanical properties or to the active vasomotor behavior of the carotid arteries. This point could be investigated by testing treated vessels with different vasodilators and vasoconstrictors to isolate the contribution of the passive and active properties of the vessels.

We speculate that the treated vessel showing divergent behavior might have already been in a later stage of pathology progression compared to the other treated vessels, for example by faster response to treatment. In fact, the increase of diameter and mean pressure and decrease of pulsatility in the other treated arteries show an intermediate behavior between untreated controls and the divergent vessel. Moreover, the degradation of the extracellular matrix in terms of presence of lacunae, which is visible in the treated vessels, results exacerbated in the divergent vessel. These observations support the consideration that the divergent vessel developed the pathology faster. In future, more experiments will be performed to assess whether this divergent behavior is possibly due to inter-subject variability.

Comparison of our outcomes with previous *ex vivo* aneurysm models cannot be directly performed. In the model by Touroo and Williams (Touroo and Williams, 2012), no native tissue was used with the limitation of lack of real tissue structure. Moreover, dilation was created artificially in the ePTFE graft. In the model used by Riches et al. (Riches et al., 2013), although damages to the extracellular matrix are shown, the *ex vivo* model was focused on SMCs phenotype in early stage aneurysms, therefore the histological findings do not result comparable. No ultrasound assessment was performed and dilation of the native vessels was not achieved, underlining the difference between our model and the other approaches.

A limitation of the present study is the use of FBS in the culture medium to provide proteins and growth factors in order to preserve expression of endothelial cell markers. However, the use of FBS rises ethical concerns because of its harvesting and collection. To overcome this limitation, we are currently looking into chemically-defined serum-free medium compositions in order to replace the use of FBS.

Currently, no blood is included in the circulation and therefore blood cells do not contribute to the aneurysm development. This reveals that the pathological modifications that were observed are to be ascribed to the stiffening and not to blood cells (e.g. inflammatory cells) which are believed to play a major role in aneurysm pathogenesis (Upchurch and Criado, 2009). For this reason, this model provides an interesting method to explore the specific contribution of stiffening, inflammation and other factors to aneurysm pathogenesis and pathophysiology. The absence of inflammatory contribution in the *ex vivo* system can be considered as a disadvantage since it is believed that inflammation has an important role in aneurysm pathogenesis. At the same time, in our study it can be seen as an advantage because our aim was to prove that the stiffening of the vascular tissue is the main cause and trigger of the aneurysm induction. To overcome potential differences in the translation between *in vivo* and *ex vivo*, in future studies, it might be interesting to investigate the combination of the effect of stiffening and presence of inflammatory contribution by, for example, adding circulating cells in the culture medium. In fact, in separate studies, not described in this paper, we have included white blood cells (e.g. monocytes) in the *ex vivo* vascular bioreactor and we demonstrated that the presence of the circulating monocytes significantly improved the healing process in the intimal layer after denudation with a significant difference compared to vessels cultured without the monocytes, demonstrating the possibility and efficacy of including circulating cells in the medium. In addition, in all *ex vivo* models using blood there is a need for anticoagulation therapies which does not represent a completely physiological conditions since, for example, it has an effect on the endothelial layer. On the other hand, the replacement of the culturing medium with blood in the system could be interesting to investigate thrombus formation, applications like aneurysms coiling and to be able to better compare histological results to *in vivo* data.

The feasibility of assessing endovascular devices in our *ex vivo* aneurysm-like model was demonstrated in a pilot study. The *ex vivo* vascular bioreactor showed to be suitable for sterile insertion, deployment and culture of a stent graft in native vessels, with an easier procedure compared to *in vivo* animal studies and allowing for daily analyses which are usually not possible in animal experimentation. Moreover, results showed a slower aneurysm progression compared to Rose Bengal-ultrasound treated arteries without stent graft implanted. These outcomes provide the first insight in testing a medical device in an *ex vivo* pathological model, bringing *ex vivo* models closer to the real clinical settings and possibly leading to reduction of *in vivo* animal studies. However, more studies will be needed to let the true pathology evolve further before actually being able to study these interventions. This pilot study paves the road for testing devices for longer periods that would allow an easier comparison with *in vivo* human and animal data and for assessing novel devices and treatment approaches, such as pharmaco-kinetics and scaffold-cell interaction studies in *in situ* tissue engineering approaches, possibly by partly modifying the system or the device insertion.

In conclusion, this study first demonstrates that Rose Bengal activated by ultrasound induces stiffening of porcine carotid arteries. This method could be further explored for applications where photo-activation is not eligible, for example for in situ collagen crosslinking in case of deep tissue which cannot be reached by light non-invasively. Moreover, this study demonstrates that stiffening of porcine carotid arteries using sono-activated Rose Bengal can be used to induce aneurysmal characteristics in cultured carotid arteries similar to the *in vivo* pathology. This model provides a promising tool to reduce the need of *in vivo* animal experiments for studying aneurysm onset and progression and testing early stage devices or drugs.

References

Barton, M., Piller, S. C., Mahns, D. A. et al. (2012). In vitro cell compatibility study of rose bengal-chitosan adhesives. *Lasers in Surgery and Medicine*, *44*(9), 762–768. doi:10.1002/lsm.22076

Bekesi, N., Gallego-Muñoz, P., Ibarés-Frías, L. et al. (2017). Biomechanical changes after in vivo collagen cross-linking with rose bengal–green light and riboflavin-UVA. *Investigative Ophthalmology and Visual Science*, *58*(3), 1612–1620. doi:10.1167/iovs.17-21475

Boekhoven, R. W., Rutten, M. C. M., van Sambeek, M. R. et al. (2014). Echo-computed tomography strain imaging of healthy and diseased carotid specimens. *Ultrasound in Med. and Biol*, *40*(6), 1329–1342. doi:10.1016/j.ultrasmedbio.2013.11.026

Campa, J. S., Greenhalgh, R. M., and Powell, J. T. (1987). Elastin degradation in abdominal aortic aneurysms. *Atherosclerosis*, *65*, 13–21. doi:10.1016/0021-9150(87)90003-7

Carmo, M., Colombo, L., Bruno, A. et al. (2002). Alteration of Elastin, Collagen and their Cross-links in Abdominal Aortic Aneurysms. *Eur J Vasc Endovasc Surg*, *23*(6), 543–549. doi:10.105 /ejvs.2002.1620

Chen, X., Wang, J., Hou, J. et al. (2009). Extracellular matrix metalloproteinase inducer (EMMPRIN) is present in smooth muscle cells of human aneurysmal aorta and is induced by angiotensin II *in vitro*. *Clinical Science*, *116*(11), 819–826. doi:10.1042/CS20080235

Cherfan, D., Verter, E. E., Melki, S. et al. (2013). Collagen cross-linking using rose bengal and green light to increase corneal stiffness. *Investigative Ophthalmology and Visual Science*, *54*(5), 3426–3433. doi:10.1167/iovs.12-11509

Czerski, A., Bujok, J., Gnus, J. et al. (2013). Experimental methods of abdominal aortic aneurysm creation in swine as a large animal model. *Journal of Physiology and Pharmachology*, *64*(2), 185–192.

Gandhi, R. H., Irizarry, E., Cantor, J. O. et al. (1994). Analysis of elastin cross-linking and the connective tissue matrix of abdominal aortic aneurysms. *Surgery*, *115*(5), 617–620.

García, A., Martínez, M. A., and Peña, E. (2012). Viscoelastic properties of the passive mechanical behavior of the porcine carotid artery: Influence of proximal and distal positions. *Biorheology*, *49*(4), 271–288. doi:10.3233/BIR-2012-0606

Gasser, T. C., Gallinetti, S., Xing, X. et al. (2012). Spatial orientation of collagen fibers in the abdominal aortic aneurysm's

wall and its relation to wall mechanics. *Acta Biomaterialia*, *8*(8), 3091–3103. doi:10.1016/j.actbio.2012.04.044

Giugliano, G., Gerardi, D., Annunziata, M. et al. (2018). Abdominal aortic aneurysm: screening and management. *Continuing Cardiology Education*, *4*(1), 34–39. doi:10.1002/cce2.73

Golledge, J. and Norman, P. E. (2011). Current status of medical management for abdominal aortic aneurysm. *Atherosclerosis*, *217*(1), 57–63. doi:10.1016/j.atherosclerosis.2011.03.006

He, C. M. and Roach, M. R. (1994). The composition and mechanical properties of abdominal aortic aneurysms. *J Vasc Surg*, *20*(1), 6–13. doi:10.1016/0741-5214(94)90169-4

Hiraoka, W., Honda, H., Feril, L. B. et al. (2006). Comparison between sonodynamic effect and photodynamic effect with photosensitizers on free radical formation and cell killing. *Ultrasonics Sonochemistry*, *13*(6), 535–542. doi:10.1016/j.ultsonch.2005.10.001

Isenburg, J. C., Simionescu, D. T., Starcher, B. C. et al. (2007). Elastin stabilization for treatment of abdominal aortic aneurysms. *Circulation*, *115*(13), 1729–1737. doi:10.1161/CIRCULATIONAHA.106.672873

Johnston, K. W., Rutherford, R. B., Tilson, M. D. et al. (1991). Suggested standards for reporting on arterial aneurysms. *J Vasc Surg*, *13*(3), 452–458. doi:10.1067/mva.1991.26737

Lauto, A., Mawad, D., Barton, M. et al. (2010). Photochemical tissue bonding with chitosan adhesive films. *BioMedical Engineering Online*, *9*, 47. doi:10.1186/1475-925X-9-47

Li, J., Bao, X., Li, Y. et al. (2016). Study of the functional mechanisms of osteopontin and chemokine-like factor 1 in the development and progression of abdominal aortic aneurysms in rats. *Experimental and Therapeutic Medicine*, *12*, 4007–4011. doi:10.3892/etm.2016.3891

Lindeman, J. H. N., Ashcroft, B. A., Beenakker, J. M. et al. (2010). Distinct defects in collagen microarchitecture underlie vessel-wall failure in advanced abdominal aneurysms and aneurysms in Marfan syndrome. *PNAS*, *107*(2), 862–865. doi:10.1073/pnas.0910312107

Loizou, C. P., Pattichis, C. S., Member, S. et al. (2009). Manual and Automated Media and Intima Thickness Measurements of the Common Carotid Artery. *IEEE*, *56*(5). doi:10.1109/TUFFC.2009.1130

Lysgaard Poulsen, J., Stubbe, J., and Lindholt, J. (2016). Animal Models Used to Explore Abdominal Aortic Aneurysms : A Systematic Review. *European Journal of Vascular and Endovascular Surgery*, *52*(4), 487–499. doi:10.1016/j.ejvs.2016.07.004

MacSweeney, S. T. R., Young, Y., Greenhalgh, R. M. et al. (1992). Mechanical properties of the aneurysmal aorta. *Br. J. Surg.*, *79*(12), 1281–1284. doi:10.1002/bjs.1800791211

Mao, N., Gu, T., Shi, E. et al. (2015). Phenotypic switching of vascular smooth muscle cells in animal model of rat thoracic aortic aneurysm. *Interactive Cardiovascular and Thoracic Surgery*, *21*(1), 62–70. doi:10.1093/icvts/ivv074

McGee, G. S., Baxter, B. T., Shively, V. P. et al. (1991). Aneurysm or occlusive disease--factors determining the clinical course of atherosclerosis of the infrarenal aorta. *Surgery*, *110*(2), 370–376.

Nakonechny, F., Nisnevitch, M., Nitzan, Y. et al. (2013). Sonodynamic Excitation of Rose Bengal for Eradication of Gram-Positive and Gram- Negative Bacteria Sonodynamic Excitation of Rose Bengal for Eradication of Gram-Positive and Gram-Negative Bacteria. *BioMed Research International*. doi:10.1155/2013/684930

Nordon, I. M., Hinchliffe, R. J., Loftus, I. M. et al. (2011). Pathophysiology and epidemiology of abdominal aortic aneurysms. *Nat. Rev. Cardiol.*, *8*(2), 92–102. doi:10.1038/nrcardio.2010.180

Nuki, Y., Tsou, T.-L., Kurihara, C. et al. (2009). Elastase-induced intracranial aneurysms in hypertensive mice. *Hypertension*, *54*(6), 1337–1344. doi:10.1161/HYPERTENSIONAHA.109.138297

O'Neill, A. C., Winograd, J. M., Zeballos, J. L. et al. (2007). Microvascular anastomosis using a photochemical tissue bonding technique. *Lasers in Surgery and Medicine*, *39*(9), 716–722. doi:10.1002/lsm.20548

Patelis, N., Moris, D., Schizas, D. et al. (2017). Animal Models in the Research of Abdominal Aortic Aneurysms Development. *Physiol Res*, *66*, 899–915.

Ren, W., Liu, Y., Wang, X. et al. (2016). β-Aminopropionitrile monofumarate induces thoracic aortic dissection in C57BL/6 mice. *Scientific Reports*, *6*, 1–7. doi:10.1038/srep28149

Riches, K., Angelini, T. G., Mudhar, G. S. et al. (2013). Exploring smooth muscle phenotype and function in a bioreactor model of abdominal aortic aneurysm. *Journal of Translational Medicine*, *11*(1), 208. doi:10.1186/1479-5876-11-208

Rizzo, R. J., McCarthy, W. J., Dixit, S. N. et al. (1989). Collagen types and matrix protein content in human abdominal aortic aneurysms. *J Vasc Surg*, *10*, 365–373. doi:10.1016/0741-5214(89)90409-6

Robertson, A. R., Duan, X., Aziz, K. M. et al. (2015). Diversity in the Strength and Structure of Unruptured Cerebral Aneurysms. *Annals of Biomedical Engineering*, *43*(7), 1502–1515. doi:10.1007/s10439-015-1252-4

Roy, S., Silacci, P., and Stergiopulos, N. (2005). Biomechanical properties of decellularized porcine common carotid arteries. *Am J Physiol Heart Circ Physiol*, *289*(4), 1567–1576. doi:10.1152/ajpheart.00564.2004

Salinas, H. M., Khan, S. I., McCormack, M. C. et al. (2017). Prevention of vein graft intimal hyperplasia with photochemical tissue passivation. *Journal of Vascular Surgery*, *65*(1), 190–196. doi:10.1016/j.jvs.2015.11.049

Sokolis, D. P., Sassani, S., Kritharis, E. P. et al. (2011). Differential histomechanical response of carotid artery in relation to species and region: Mathematical description accounting for elastin and collagen anisotropy. *Medical and Biological Engineering and Computing*, *49*(8), 867–879. doi:10.1007/s11517-011-0784-5

Sonesson, B., Hansen, F., and Lanne, T. (1997). Abdominal aortic aneurysm: A general defect in the vasculature with focal manifestations in the abdominal aorta? *Journal of Vascular Surgery*, *26*(2), 247–254. doi:10.1016/S0741-5214(97)70185-X

Tanweer, O., Wilson, T. A., Metaxa, E. et al. (2014). A Comparative Review of the Hemodynamics and Pathogenesis of Cerebral and Abdominal Aortic Aneurysms: Lessons to Learn From Each Other. *Journal of Cerebrovascular and Endovascular Neurosurgery*, *16*(4), 335–349. doi:10.1136/neurintsurg-2014-011343.83

Touroo, J. S., and Williams, S. K. (2012). A tissue-engineered aneurysm model for evaluation of endovascular devices. *Journal*

of Biomedical Materials Research - Part A, *100A*(12), 3189–3196. doi:10.1002/jbm.a.34256

Trachet, B., Piersigilli, A., Fraga-Silva, R. A. et al. (2016). Ascending Aortic Aneurysm in Angiotensin II-Infused Mice: Formation, Progression, and the Role of Focal Dissections. *Arteriosclerosis, Thrombosis, and Vascular Biology*, *36*(4), 673–681. doi:10.1161/ATVBAHA.116.307211

Upchurch, G. R., and Criado, E. (2009). *Aortic Aneurysms - Pathogenesis and treatment*. (G. R. Upchurch and E. Criado, Eds.). Humana Press. doi:10.1007/978-1-60327-204-9

Vande Geest, J. P., Sacks, M. S., and Vorp, D. A. (2006). The effects of aneurysm on the biaxial mechanical behavior of human abdominal aorta. *Journal of Biomechanics*, *39*(7), 1324–1334. doi:10.1016/j.jbiomech.2005.03.003

Vanerio, N., Stijnen, M., de Mol, B. A., and Kock, L. M. (2019). Biomedical Applications of Photo- and Sono-Activated Rose Bengal: A Review. *Photobiomodulation, Photomedicine, and Laser Surgery*, 1–13. doi:10.1089/photob.2018.4604

Wågsäter, D., Paloschi, V., Hanemaaijer, R. et al. (2013). Impaired collagen biosynthesis and cross-linking in aorta of patients with bicuspid aortic valve. *Journal of the American Heart Association*, *2*(1), 1–11. doi:10.1161/JAHA.112.000034

Xu, N., Yao, M., Farinelli, W. A. et al. (2015). Light-activated sealing of skin wounds. *Lasers in Surgery and Medicine*, *47*(1), 17–29. doi:10.1002/lsm.22308

Conflict of interest

Noemi Vanerio, Marco Stijnen and Linda M. Kock are employees of LifeTec Group BV. Bas A. J. M. de Mol is an advisor of LifeTec Group BV.

Acknowledgements

This work was supported by the European Commission within the Horizon 2020 Framework through the MSCA-ITN-ETN European Training Networks (project number 642458).